

Oxygen adsorption on Ag/Si(111)-7×7 surfaces

Zhen Zhang, Jian Jiao, Zhiqian Jiang, Dali Tan, Qiang Fu,^{a),b)} and Xinhe Bao^{a),c)}
State Key Laboratory of Catalysis, Dalian Institute of Chemical Physics, The Chinese Academy
of Sciences, Dalian 116023, People's Republic of China

Xi Liu,^{d)} Jinfeng Jia,^{d)} and Qikun Xue^{d)}
State Key Laboratory for Surface Physics, Institute of Physics, The Chinese Academy of Sciences,
Beijing 100080, People's Republic of China

(Received 29 May 2007; accepted 24 October 2007; published 14 December 2007)

The growth of Ag clusters on Si(111)-7×7 surfaces was studied by scanning tunneling microscopy (STM), ultraviolet photoelectron spectroscopy, and x-ray photoelectron spectroscopy (XPS). A shift in the Ag 3*d* binding energy and a noticeable change in the valence-band structure reveal a significant modification of the electronic states of the Si(111)-7×7 surface and the dispersed Ag clusters, which had a strong dependence on the coverage of Ag. Furthermore, these Ag clusters deposited on the Si surface alter the behavior of oxygen adsorption on the Si(111)-7×7 surface. As evidenced by XPS, the presence of Ag inhibits the adsorbed surface oxygen species, the ins-ins and ad-ins oxygen, in which “ad” denotes an O atom bonding on top of the Si adatom and “ins” denotes an O atom inserted into a Si adatom back bond. The STM and high-resolution electron energy loss spectroscopy results show that the ins-ins oxygen species are more significantly suppressed by the Ag clusters compared to the ad-ins oxygen.

© 2008 American Vacuum Society. [DOI: 10.1116/1.2816938]

I. INTRODUCTION

Metal nanoclusters have been intensively studied in the past decades because of their wide application in the fields of microelectronics and industrial catalysis.^{1,2} The numerous novel properties of nanoclusters also attract fundamental research. Many research efforts in metal clusters have focused on model systems that consist of nanoclusters supported on well-defined surfaces, and such model systems with *in situ* surface analytic techniques greatly enhance the understanding of their unique physical and chemical properties.

One key aspect of the model systems is the control of growth of nanoclusters on certain surfaces. Some sophisticated preparation techniques, e.g., size-selected cluster deposition^{3,4} and electron-beam lithography,⁵ have been developed and improved in the last decades. Among them, self-organized growth mediated by periodic templates has been demonstrated to be an effective approach for obtaining ordered metal nanoclusters, and the various periodic templates, such as boron nitride nanomeshes,⁶ Au(788) surface,⁷ and surfaces with periodic strain-relief patterns,⁸ have been exploited. The Si(111)-7×7 surface, which consists of large (~2.7 nm) triangular half-unit cells (HUCs), has been considered as a natural template for growing ordered metal clusters, and some interesting artifacts, showing the ordered arrays of Al, Ga, and In nanoclusters on Si(111)-7×7 surfaces have been successfully created by Xue and co-workers.^{9,10} Silver appears as an important catalyst because it is active in

the catalytic processes of ethylene oxidation and methanol selective oxidation. Also, silver's size and structure show a strong influence on its catalytic reactivity and selectivity. For example, adsorption of O₂ on Ag clusters grown on TiO₂(110) (Ref. 11) and graphite surfaces^{12,13} is closely related to the Ag clusters size. To better understand the mechanism of Ag-related catalysis, it is often useful to study the chemical and physical properties of Ag clusters in a well-controlled model system such as Ag/Si(111)-7×7 system. Ag is nonreactive on Si(111)-7×7 at low temperatures (<500 K), and adsorption of Ag leaves the 7×7 reconstruction unchanged.^{14,15} Therefore, Ag/Si(111)-7×7 is one of the ideal model systems for studying the controlled growth of metal clusters on Si(111)-7×7. The nucleation of Ag clusters on Si(111)-7×7 has been carefully investigated by different research groups.^{16–20} However, the surface adsorption properties of the Ag/Si(111)-7×7 system were rarely addressed.²¹

In the present work, we concentrate on the model systems of Ag/Si, and address the controlled growth of Ag clusters on the Si(111) surface and the induced characters to the interaction with oxygen. Scanning tunneling microscopy (STM), ultraviolet photoelectron spectroscopy (UPS), and x-ray photoelectron spectroscopy (XPS) have been used to investigate the surface morphology and electronic structure, and the reactivity of the Ag/Si(111)-7×7 surfaces to O₂ was characterized by STM and high-resolution electron energy loss spectroscopy (HREELS).

II. EXPERIMENT

Experiments were carried out in two separated ultrahigh-vacuum (UHV) systems. One was equipped with an Omicron variable-temperature STM and evaporators. Ag deposition

^{a)} Authors to whom correspondence should be addressed.

^{b)} Electronic mail: qfu@dicp.ac.cn

^{c)} Electronic mail: xhbao@dicp.ac.cn

^{d)} Present address: Tsinghua University, Dept. of Physics, Beijing, 100084, People's Republic of China.

was performed by resistive heating in a tungsten bracket. The other was an Omicron multiprobe surface-analysis system that consists of three UHV chambers: preparation, spectroscopic, and microscopic chambers. The preparation chamber is equipped with an evaporator with integral flux monitor (Focus EFM3) for Ag deposition. The spectroscopic chamber is installed with XPS, UPS, and HREELS (LK-ELS5000), and the microscopic chamber is equipped with STM/atomic force microscopy and photoemission electron microscopy. The three chambers are connected with a transfer chamber, through which the sample can be transferred among these chambers by magnetically coupled probes without breaking the vacuum.

XPS data were acquired with Mg $K\alpha$ ($h\nu=1253.6$ eV) radiation and pass energy at 50 eV. The spectra were calibrated with the Ag $3d_{5/2}$ peak at 368.1 eV. UP spectra were recorded at normal emission with He II radiation ($h\nu=40.8$ eV), and the photoelectron peak positions were calibrated with respect to the Si(111)-7×7 Fermi level (E_F). In HREELS, the monochromatized electrons were incident at an angle of 55° with respect to the surface normal of the sample. The primary energy (E_p) was 7.2 eV. The energy resolution of the spectrometer was ~ 10 meV, which was shown from the full width at half maximum of the elastic peak. STM measurement was carried out at room temperature (RT) with a constant current mode using a homemade W tip.

The Si(111) sample (P doped) was cleaned by flashing the sample to 1200 °C for several cycles. Ag was deposited on the clean Si(111)-7×7 surfaces at RT. The flux was calibrated by counting the Ag clusters at ultralow coverage using STM. O₂ was introduced onto the sample surfaces by back-filling the chamber via a leak valve.

III. RESULTS AND DISCUSSION

A. Growth of Ag clusters on Si(111)-7×7

Figure 1 shows the STM images of Ag on Si(111)-7×7 surfaces with different Ag coverages. At very low coverage [0.005 monolayer (ML) and 0.01 ML, as shown in Figs. 1(a)–1(c)], three types of Ag clusters can be identified: type I (solid circle), type II (dotted circle), and type III (dashed circle). In case of the type I cluster, which is often located in faulted half-unit cells (FHUCs), three Si corner adatoms in the HUC are highlighted at both positive and negative bias voltages. For the type II cluster, all the six Si adatoms in the HUC are highlighted at negative bias voltage and a bright spot can be seen at positive bias [Figs. 1(a) and 1(b)]. The type III cluster shows itself as a bright spot and no specific shape can be observed at any bias voltages. The three types of Ag clusters may be attributed to monomer, dimer, and cluster containing more than two Ag atoms.^{17,18,20} The population of type I clusters decreases quickly with increasing Ag coverage, being accompanied by an increase in the population of the type II and type III clusters. At 0.12 ML Ag coverage, more atoms add into a HUC, and the type III clusters are already dominant on the surface [Fig. 1(d)]. With

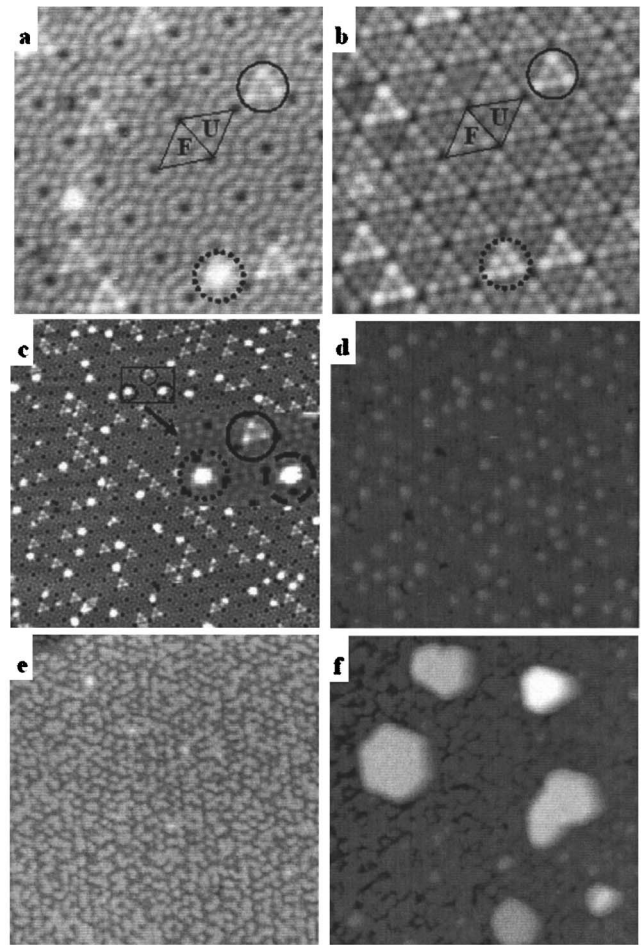


Fig. 1. STM images of Ag on Si(111)-7×7 surface with different coverages: (a) ~ 0.005 ML, 2 V, 19×19 nm²; (b) ~ 0.005 ML, -2 V, 19×19 nm²; (c) 0.01 ML, 2 V, 50×50 nm²; (d) 0.12 ML, 1.5 V, 50×50 nm²; (e) 0.6 ML, 1.5 V, 100×100 nm²; (f) 1.2 ML, 1.5 V, 100×100 nm². (a) and (b) are the same area, but acquired at different bias voltages. The triangles in (a) indicate the faulted HUC (FHUC) and unfaulted HUC (UHUC) on Si(111)-7×7 surface. The solid, dotted, and dashed circles represent types I, II, and III Ag clusters, respectively.

further Ag deposition, two of the type III clusters separated by a dimer row link up with Ag adatoms, which show a discontinuous wormlike shape in STM images;²² furthermore, a wetting layer forms [Fig. 1(e)]. Above 0.6 ML, three-dimensional (3D) islands start to grow on top of the wetting layer [Fig. 1(f)]. The results show that Ag grows on the Si(111)-7×7 surface according to the Stranski-Krastanov mode, in which formation of one or more monolayers is followed by the growth of 3D islands. The strain induced by the lattice mismatch between the Si substrate and Ag may result in the transition from the two-dimensional to 3D growth.

UP spectra taken from the Ag/Si(111) surfaces with different Ag coverages are shown in Fig. 2. For the clean Si(111)-7×7 surface, two peaks at 0.15 and 0.85 eV below E_F , labeled as S_1 and S_2 , respectively, can be attributed to the photoemission from the dangling bonds of adatoms and rest atoms on the Si(111)-7×7 surface.^{23,24} With the nucleation

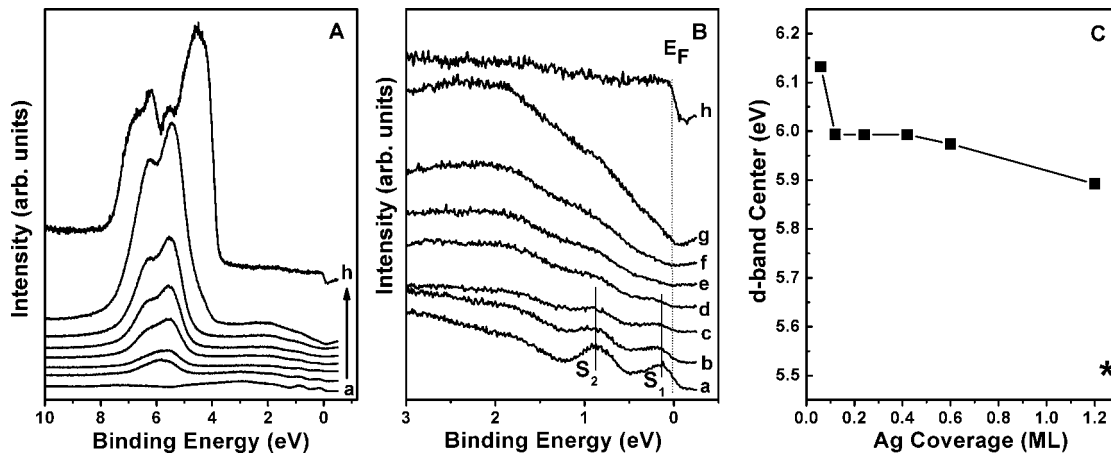


Fig. 2. [(A) and (B)] He II (40.8 eV) valence-band spectra of Ag on Si(111)-7×7 surface with different coverages: (a) 0 ML (clean Si(111)-7×7); (b) 0.06 ML; (c) 0.12 ML; (d) 0.24 ML; (e) 0.42 ML; (f) 0.6 ML; (g) 1.2 ML; (h) He II UPS of Ag(111). (C) d valence-band center as a function of Ag coverage. The asterisk (*) marks the d -band center of Ag(111) in (C).

of Ag on the surface, both S_1 and S_2 states diminish quickly [Fig. 2(B)] and this is partially due to the saturation of the dangling bonds on Si surfaces by the deposited Ag clusters.²⁵ More interestingly, the density of states (DOS) near E_F decreases as the Ag coverage increases up to 0.42 ML [from Figs. 2(B), (a)–(e)], which is accompanied by the evident suppressing of the Si surface state (S_1) near E_F . This feature indicates the nonmetallic character of Ag clusters at these coverages, which is consistent with the previous scanning tunneling spectroscopy results.¹⁴ Above 0.6 ML, DOS near E_F increases with the Ag coverage [see Figs. 2(B), (e) and (f)], which demonstrates the transition of Ag clusters toward metallic character, and the corresponding STM images confirmed the formation of the large Ag clusters, as shown in Fig. 1(f).

Compared to the Ag(111) surface [Fig. 1(h)], Ag $4d$ bands of the Ag overlayers grown on the Si(111)-7×7 surface [Figs. 1(b)–1(f)] is much narrower, which is due to the re-

duction of the coordination number in Ag nanoclusters.²⁶ At the same time, the UPS results show that the Ag $4d$ bands of the Ag nanoclusters shift to higher binding energy, which is attributed to the redistribution of valence-band states as suggested by Guzci *et al.*^{27,28} Figure 2(C) presents a plot of the Ag $4d$ band center, which was calculated following the method suggested by Mun *et al.*,²⁹ with Ag coverage. The d -band center decreases from 6.13 to 5.9 eV as the Ag coverage on the surface increases from 0.06 to 1.2 ML. The d -band center of the Ag(111) is at 5.51 eV. The shift in d -band center of metal catalysts may potentially influence their catalytic performance.³⁰

The Ag $3d$ XPS spectra were included in Fig. 3. A trivial Ag $3d_{5/2}$ peak shift in position occurs from 368.8 (at the Ag coverage of 0.06 ML) to 368.6 eV (at the Ag coverage of 0.60 ML). These values are significantly larger than that at Ag $3d_{5/2}$ with the value of 368.1 eV in bulk Ag [shown by an asterisk in Fig. 3(B)]. Both change in the $4d$ band center and

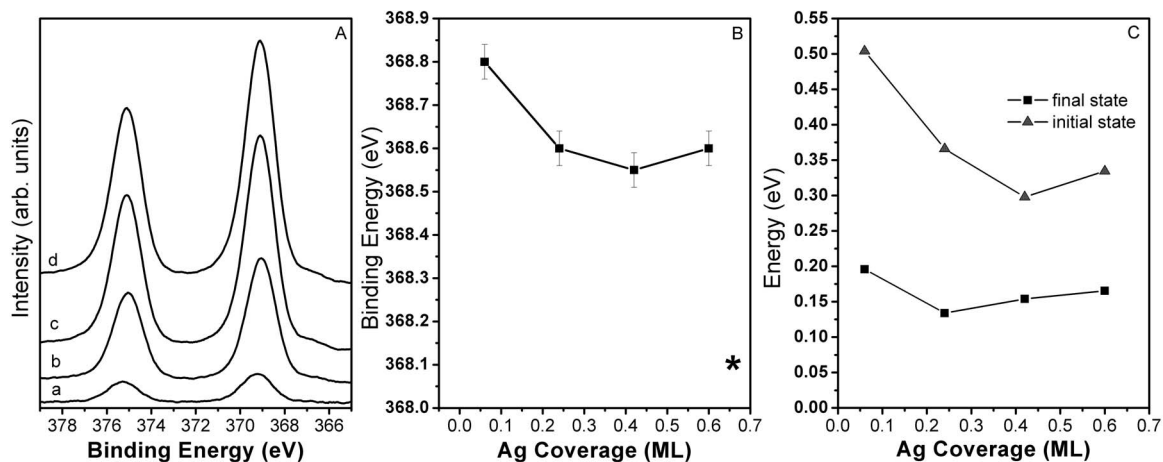


Fig. 3. (A) Ag $3d$ XPS spectra of (a) 0.06 ML, (b) 0.24 ML, (c) 0.42 ML, and (d) 0.60 ML Ag on Si(111)-7×7 surfaces; (B) Ag $3d_{5/2}$ binding energy as a function of Ag coverage; (C) initial- and final-state contributions to the Ag $3d_{5/2}$ shifts as a function of Ag coverage. The asterisk (*) indicates the Ag $3d_{5/2}$ binding energy of Ag(111) in (B).

shift of core-level binding energy (BE) of small Ag clusters in comparison to the bulk Ag surface may be attributed to the initial-state and/or final-state effects. The initial-state effect is correlated with the change in electronic structure of the metal clusters, and the final-state effect to the screening of the photoemission core holes.³¹ It is still challenging to differentiate the relative contribution of the initial- and final-state effects.^{26,32,33} Nevertheless, both contributions to the core-level shifts can be estimated using the concept of Auger parameter (α).^{33,34} Here, the Auger parameter of Ag was calculated as

$$\alpha(\text{Ag}) = E_b(\text{Ag}3d_{5/2}) + E_k(\text{Ag}M_5VV),$$

where E_b (Ag $3d_{5/2}$) is the binding energy of the Ag $3d_{5/2}$ core level and E_k (Ag M_5VV) is the kinetic energy of the Ag M_5VV Auger transition. As suggested by Luo *et al.*,^{33,34} the change in the Auger parameter of $\Delta\alpha(\text{Ag})$, defined by $\Delta\alpha = 2\Delta R$, can be used to estimate the final-state effect (ΔR) in clusters, and it is possible to separate the initial-state and final-state contributions to the BE shifts. Our Auger parameter analysis shows that the initial-state effect gives a major contribution, $\sim 70\%$ of the total ΔBE at the Ag coverage smaller than 0.6 ML [see Fig. 3(C)]. The STM results have shown that, below 0.6 ML, the silver clusters are one monolayer high and all the Ag adatoms make bonds with the surface Si atoms. The interfacial bonding and the resultant electronic interaction between Ag and Si atoms may contribute to the dominant initial-state effect.

B. Interaction of oxygen with Ag/Si(111)-7×7

The interaction of molecular oxygen with a clean silicon surface is much stronger than that with a silver surface, and the active exposure of O_2 to the Ag/Si(111)-7×7 system will result in forming different surface oxygen species relating to Si–O interaction, but no obvious existence of oxygen species concerning a Ag cluster. Although oxygen can adsorb onto silver surfaces, the low sticking coefficient of oxygen on Ag may result in little oxygen adsorbed on the Ag surfaces under these O_2 exposure conditions.³⁵ In this work, we focus on the effect of silver on the interaction of the silicon surface with oxygen. STM, HREELS, and XPS were used to uncover the structural changes and evolution of the oxygen species during oxygen exposure.

The inset in Fig. 4 displays a typical STM image of a 0.02 ML Ag/Si(111)-7×7 surface exposed to 0.05 L O_2 . Some Si adatom sites in the HUCs become either brighter or darker after O_2 adsorption. Based on the previous explanation, two such species on the O_2 -exposed Si(111)-7×7 surfaces have been ascribed to chemisorbed O_2 molecules.^{36–38} However, recent density-functional theory calculations^{39,40} and experimental studies^{41,42} excluded the existence of any molecular O_2 species at RT. It becomes acceptable currently that two atomic oxygen configurations exist at initial oxygen adsorption on the Si(111)-7×7 surface: ad-ins and ins-ins oxygen (“ad” denotes an O atom bonding on top of the Si adatom, and “ins” denotes an O atom inserted into a Si adatom back bond, Fig. 5).³⁹ The bright and dark species in STM images

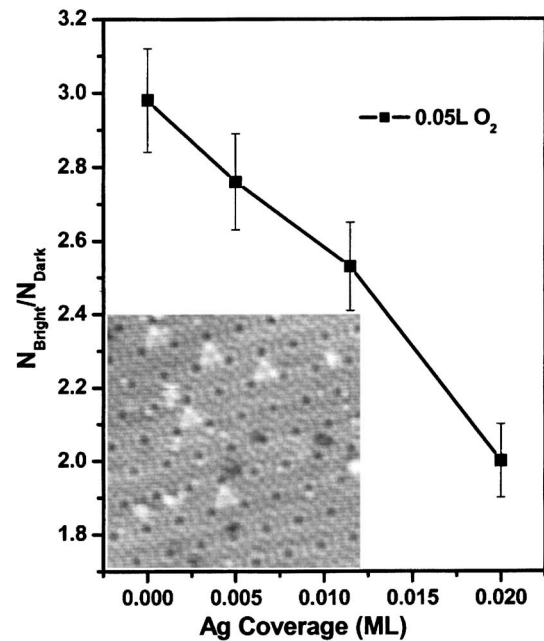


Fig. 4. The ratio of bright oxygen species to dark oxygen species on Ag/Si(111)-7×7 surface exposed to 0.05 L O_2 at different Ag coverages; Inset: the STM image of 0.02 ML Ag/Si(111) surface after exposing to 0.05 L O_2 .

correspond to the ins-ins and ad-ins oxygen configurations, respectively.^{39,43} Figure 4 is the plot of the ratio of ins-ins to ad-ins oxygen species on Ag/Si(111)-7×7 surfaces as a function of Ag coverage after exposure of 0.05 L O_2 . The numbers of ins-ins and ad-ins oxygen species are obtained after carefully counting of bright and dark species in several STM images. A clear decrease in the ratio of ins-ins to ad-ins oxygen species occurs when more Ag atoms are located on the surface (Ag coverage < 0.02 ML). This means that the presence of Ag clusters affects the surface chemisorbed oxygen species on Si(111)-7×7, and the ins-ins oxygen configuration is inhibited by the Ag clusters. The previous *in situ* STM investigations also indicate that ins-ins oxygen could be converted to ad-ins oxygen by the Ag clusters on the O_2 -exposed Ag/Si(111)-7×7 surfaces.²¹ Based on these results, the microscopic interaction between Ag clusters and the surface Si–O groups on the O_2 -exposed Ag/Si surface can be illustrated by the schematics in Fig. 5, which shows that the ins-ins oxygen configuration is less stable on Si(111)-7×7 in the presence of Ag clusters.

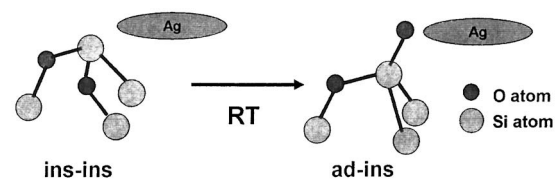


Fig. 5. Schematic of the change in the oxygen configuration from ins-ins to ad-ins in the presence of Ag clusters.

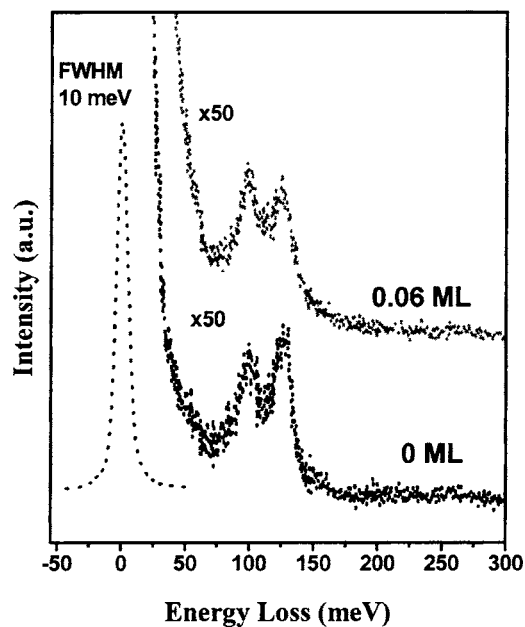


FIG. 6. HREELS spectra from both bare Si(111)-7×7 surface and 0.06 ML Ag/Si(111)-7×7 surface exposed to 0.68 L O₂.

This mechanism summarized by the Ag/Si model system may help us to understand the interaction between metal adatoms and silica surfaces. Lopez *et al.*⁴⁴ investigated the interaction of Cu and Pd atoms on regular and defect sites of the SiO₂ surface by theoretical calculations. They found that the nonbridging species ($\equiv\text{Si}-\text{O}\cdot$) are the most reactive sites on the silica surface. Recently, gold atoms were also found to be trapped at $\equiv\text{Si}-\text{O}\cdot$ and $\equiv\text{Si}-\text{O}^-$ defect sites on amorphous silica.⁴⁵ As we discussed above, Ag clusters interact more strongly with ad-ins oxygen species and could convert the oxygen configuration from the ins oxygen (Si-O-Si) to the ad oxygen (Si-O) (as illustrated in Fig. 5). This STM result gives a direct atomic image showing evidence that metal adatoms try to bond with surface-nonbridging oxygen species ($\equiv\text{Si}-\text{O}$), rather than with surface-bridging oxygen species (Si-O-Si).

HREEL spectra from Si(111)-7×7 and 0.06 ML Ag/Si(111)-7×7 surfaces after exposing to 0.68 L O₂ are given in Fig. 6. Two dominant features are observed at ~99 and ~127 meV, and both of them are from the Si-O vibration.⁴⁶ The 127 meV peak is attributed to Si-O-Si asymmetric stretching vibration, and the bond formation is considered to occur by breaking the Si-Si bond in the Si substrate (ins oxygen configuration).⁴⁷⁻⁵⁰ The 99 meV peak is due to a Si-O stretching vibration that is associated with a single bond formed between atomic oxygen and a silicon adatom (ad oxygen configuration).⁴⁷⁻⁵⁰ At the 0.06 ML Ag/Si(111)-7×7 surface, the HREEL spectrum shows the same features, but more enhancement of the 99 meV peak relative to the 127 meV peak. The HREELS data further support the STM results (Figs. 4 and 5), showing that the presence of Ag clusters changes the relative population of the ins-ins oxygen to the ad-ins oxygen species.

The O₂ adsorption on Ag/Si(111)-7×7 surfaces has been investigated as a function of O₂ exposure and Ag coverage using XPS. Figure 7(a) shows the variation of ratio of XPS O 1s to Si 2p intensity ($I_{\text{O}}/I_{\text{Si}}$) with O₂ exposure at different Ag coverage. It can be seen that $I_{\text{O}}/I_{\text{Si}}$ always increases sharply in the range of 0.06–2.22 L O₂; then, the surface is nearly saturated by oxygen with the oxygen exposure ranging from 2.22 to 48.37 L. This result can be easily understood in that a larger amount of O₂ exposure to the Ag/Si surfaces produces more chemisorbed oxygen on the surfaces. Figure 7(b) presents $I_{\text{O}}/I_{\text{Si}}$ of Ag/Si(111)-7×7 surfaces as a function of Ag coverage at 0.68 and 48.4 L O₂ exposures, respectively. The plots demonstrate that a small amount of Ag adsorption (from 0.06 to 0.42 ML) has induced a decrease to ~70% in O₂ adsorption on the Si(111)-7×7 surface. At 0.6 ML Ag/Si(111)-7×7, $I_{\text{O}}/I_{\text{Si}}$ decreases down to ~40%. In contrast to the enhancement of oxygen adsorption on Si by Cu deposition,⁴⁹ our result indicates that Ag can suppress the oxygen adsorption on Si(111), in particular, the formation of ins-ins oxygen species. Because even 0.06 ML Ag could reduce the surface oxygen adsorption capacity to 70%, we suggest that the inhibition effect is mainly due to the electronic factor. As we have discussed in the last section, adsorption of

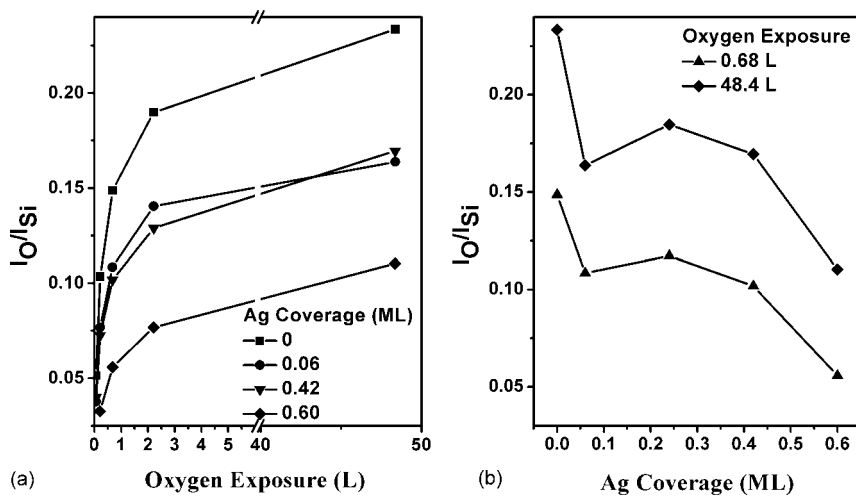


FIG. 7. XPS intensity ratio $I(\text{O } 1s)/I(\text{Si } 2p)$ on Ag/Si(111) (a) as a function of oxygen exposure at RT at various Ag coverages and (b) as a function of Ag coverage at 0.68 and 48.4 L O₂ exposures, respectively.

Ag clusters induces a large change in both Si surface states and DOS at E_F , thus, it is expected that the modification of the surface electronic structure contributes to the decrease in the reactivity of the Si surface to O_2 . At higher Ag coverage, the Ag inhibition may be due to both the electronic factor and stereoblocking of the adsorption sites. Similar phenomena have been found in the STM study of the oxidation of Au/Si(111)-7×7 surfaces by Kishi *et al.*⁵¹

IV. CONCLUSIONS

Various Ag clusters, i.e., monomers, dimers, and small Ag islands, have been obtained on Si(111)-7×7 surfaces at RT. The electronic structure of the composite system, including the Si surface states and DOS near E_F , was seen to be modulated by the Ag coverage. The existence of Ag clusters strongly influences the surface adsorption of O_2 on Si. It is found that Ag clusters inhibit the formation of ad-ins oxygen and, more significantly, ins-ins oxygen species, which distinctly changes the relative population of ins-ins oxygen to ad-ins oxygen species on the surfaces. This inhibition effect has been attributed to Ag-induced change in the Si surface electronic state at low Ag coverage and the stereoblocking of adsorption sites at high Ag coverage.

ACKNOWLEDGMENT

This work was supported financially by the National Natural Science Foundation of China (Nos. 90206036, 20573107, and 20603037).

¹K.-H. Meiwes-Broer, *Metal Clusters at Surfaces: Structure, Quantum Properties, Physical Chemistry* (Springer, Berlin, 2000).

²C. Binns, Surf. Sci. Rep. **44**, 1 (2001).

³X. Tong, L. Benz, P. Kemper, H. Metiu, M. T. Bowers, and S. K. Buratto, J. Am. Chem. Soc. **127**, 13516 (2005).

⁴L. Benz, X. Tong, P. Kemper, Y. Lilach, A. Kolmakov, H. Metiu, M. T. Bowers, and S. K. Buratto, J. Chem. Phys. **122**, 081102 (2005).

⁵J. Grunes, J. Zhu, E. A. Anderson, and G. A. Somorjai, J. Phys. Chem. B **106**, 11463 (2002).

⁶M. Corso, W. Auwärter, M. Muntwiler, A. Tamai, T. Greber, and J. Osterwalder, Science **303**, 217 (2004).

⁷V. Repain, G. Baudot, H. Ellmer, and S. Rousset, Europhys. Lett. **58**, 730 (2002).

⁸H. Brune, M. Giovannini, K. Bromann, and K. Kern, Nature (London) **394**, 451 (1998).

⁹J.-L. Li, J.-F. Jia, X.-J. Liang, X. Liu, J.-Z. Wang, Q.-K. Xue, Z.-Q. Li, J. S. Tse, Z. Zhang, and S. B. Zhang, Phys. Rev. Lett. **88**, 066101 (2002).

¹⁰J. Jia, J.-Z. Wang, X. Liu, Q.-K. Xue, Z.-Q. Li, Y. Kawazoe, and S. B. Zhang, Appl. Phys. Lett. **80**, 3186 (2002).

¹¹X. Lai, T. P. St. Clair, and D. W. Goodman, Faraday Discuss. **114**, 279 (1999).

¹²V. I. Bukhtiyarov, A. F. Carley, L. A. Dollard, and M. W. Roberts, Surf. Sci. **381**, L605 (1997).

¹³H. Hövel, B. Grimm, M. Bödecker, K. Fieger, and B. Reihl, Surf. Sci.

463, L603 (2000).

¹⁴S. Tosch and H. Neddermeyer, Phys. Rev. Lett. **61**, 349 (1988).

¹⁵K. J. Wan, X. F. Lin, and J. Nogami, Phys. Rev. B **47**, 13700 (1993).

¹⁶A. Shibata, Y. Kimura, and K. Takayanagi, Surf. Sci. **303**, 161 (1994).

¹⁷H. Hirayama, H. Okamoto, and K. Takayanagi, Phys. Rev. B **60**, 14260 (1999).

¹⁸T. Jarolímek, J. Mysliveček, P. Šmilauer, and I. Ošťádal, Surf. Sci. **482–485**, 386 (2001).

¹⁹J. Mysliveček, P. Sobotík, I. Ošťádal, T. Jarolímek, and P. Šmilauer, Phys. Rev. B **63**, 045403 (2001).

²⁰C. Zhang, G. Chen, K. Wang, H. Yang, T. Su, C. T. Chan, M. M. T. Loy, and X. Xiao, Phys. Rev. Lett. **94**, 176104 (2005).

²¹J. Jiao, M. Pan, Q. Xue, and X. Bao, Chin. J. Catal. **24**, 433 (2003).

²²P. Sobotík, I. Ošťádal, and P. Kocán, Surf. Sci. **507–510**, 389 (2002).

²³J. E. Northrup, Phys. Rev. Lett. **57**, 154 (1986).

²⁴R. J. Hamers, R. M. Tromp, and J. E. Demuth, Phys. Rev. Lett. **56**, 1972 (1986).

²⁵A. L. Wachs, A. P. Shapiro, T. C. Hsieh, and T.-C. Chiang, Phys. Rev. B **33**, 1460 (1986).

²⁶G. K. Wertheim, S. B. DiCenzo, and D. N. E. Buchanan, Phys. Rev. B **33**, 5384 (1986).

²⁷Z. Pászti, G. Pető, Z. E. Horváth, A. Karacs, and L. Guzzi, Solid State Commun. **107**, 329 (1998).

²⁸L. Guzzi, G. Pető, A. Beck, K. Frey, O. Geszti, G. Molnár, and C. Daróczy, J. Am. Chem. Soc. **125**, 4332 (2003).

²⁹B. S. Mun, C. Lee, V. Stamenkovic, N. M. Markovic, and P. N. Ross, Jr., J. Chem. Phys. **122**, 184712 (2005).

³⁰B. Hammer and J. K. Nørskov, Adv. Catal. **45**, 71 (2000).

³¹C. R. Henry, Surf. Sci. Rep. **31**, 235 (1998).

³²I. Lopez-Salido, D. C. Lim, R. Dietsche, N. Bertram, and Y. D. Kim, J. Phys. Chem. B **110**, 1128 (2006).

³³K. Luo, X. Lai, C.-W. Yi, K. A. Davis, K. K. Gath, and D. W. Goodman, J. Phys. Chem. B **109**, 4064 (2005).

³⁴Y. Wu, E. Garfunkel, and T. E. Madey, J. Vac. Sci. Technol. A **14**, 1662 (1996).

³⁵C. T. Campbell, Surf. Sci. **157**, 43 (1985).

³⁶I.-S. Hwang, R.-L. Lo, and T. T. Tsong, Surf. Sci. **399**, 173 (1998).

³⁷G. Dujardin, A. Mayne, G. Comtet, L. Hellner, M. Jamet, E. Le Goff, and P. Millet, Phys. Rev. Lett. **76**, 3782 (1996).

³⁸R. Martel, P. Avouris, and I.-W. Lyo, Science **272**, 385 (1996).

³⁹S.-H. Lee and M.-H. Kang, Phys. Rev. Lett. **82**, 968 (1999).

⁴⁰S.-H. Lee and M.-H. Kang, Phys. Rev. B **61**, 8250 (2000).

⁴¹F. Matusi, H. W. Yeom, K. Amemiya, K. Tono, and T. Ohta, Phys. Rev. Lett. **85**, 630 (2000).

⁴²K.-Y. Kim, T.-H. Shin, S.-J. Han, and H. Kang, Phys. Rev. Lett. **82**, 1329 (1999).

⁴³H. Okuyama, T. Yamada, and T. Aruga, Jpn. J. Appl. Phys., Part 1 **44**, 5362 (2005).

⁴⁴N. Lopez, F. Illas, and G. Pacchioni, J. Am. Chem. Soc. **121**, 813 (1999).

⁴⁵J.-M. Antonietti, M. Michalski, U. Heiz, H. Jones, K. H. Lim, N. Rösch, A. D. Vitto, and G. Pacchioni, Phys. Rev. Lett. **94**, 213402 (2005).

⁴⁶P. A. Thiry, M. Liehr, J. J. Pireaux, R. Sporken, R. Caudano, J. P. Vigneron, and A. A. Lucas, J. Vac. Sci. Technol. B **3**, 1118 (1985).

⁴⁷K. Edamoto, Y. Kubota, H. Kobayashi, M. Onchi, and M. Nishijima, J. Chem. Phys. **83**, 428 (1985).

⁴⁸M. Nishijima, K. Edamoto, Y. Kubota, H. Kobayashi, and M. Onchi, Surf. Sci. **158**, 422 (1985).

⁴⁹P. J. Møller and J.-W. He, J. Vac. Sci. Technol. A **5**, 996 (1987).

⁵⁰K. Sakamoto, S. Suto, and W. Uchida, Surf. Sci. **357–358**, 514 (1996).

⁵¹K. Kishi, M. Daté, and M. Haruta, Surf. Sci. **486**, L475 (2001).